Acta Metall. Sin. (Engl. Lett.), 2018, **31**, 337–350
https://doi.org/10.1007/s40195-017-0672-6

Influence of Processing Parameters on Microstructural Evolution and Tensile Properties for 7075 Al Alloy Prepared by an ECAP-Based SIMA Process

Jin-Long Fu[1] · Hong-Jun Jiang[2] · Kai-Kun Wang[1]

Received: 30 June 2017 / Revised: 31 August 2017 / Published online: 9 November 2017

Abstract A modified strain-induced melt activation (SIMA) process consisting of homogenization, equal-channel angular pressing (ECAP) and subsequent heating to the semisolid temperatures was introduced to prepare the 7075 aluminum alloy with superior thixotropic behaviors. The effects of both the homogenization and the number of ECAP passes, as well as the isothermal temperatures on the microstructural evolution, were investigated. The results indicate that ideal microstructure wherein fine and globular solid grains surrounded by uniform liquid films can be achieved through ECAP deformation–recrystallization mechanism. Increasing the number of ECAP passes accelerates the recrystallization of strained grains, thus reducing the average grain size and improving the grain sphericity. Moreover, higher holding temperatures and prolonged soaking time can improve the growth of the solid grains. Two main coarsening mechanisms, viz. coalescence and Ostwald ripening, contribute to the growth of the solid grains simultaneously and independently. The tensile strength of the 7075 alloys after four-pass ECAP-based SIMA and T6 heat treatment is relatively lower than the as-received billet, while the elongation of SIMA processed samples is much higher than that of as-received ones. Increasing the number of ECAP passes improves the tensile strength for alloys with and without T6 treatment due to the fine grain strengthening mechanism.

KEY WORDS: Semisolid; Aluminum; Equal-channel angular pressing; Microstructural evolution; Tensile property

1 Introduction

High-strength, high-performance Al–Zn–Mg–Cu alloy has already been widely used in the industries of aerospace and automobiles owing to the highest mechanical properties of aluminum alloys [1]. 7xxx aluminum alloy has been studied by means of traditional casting, plastic deformation and powder metallurgy [2]. However, problems of hot cracks, high deformation resistance, low relative density and high cost hinder the commercial use of 7075 alloys [3].

Semisolid processing (SSP), as a near net-shape manufacturing technology, is of high economic and technical interest. SSP combines the advantages of casting and forging [4] and has been successfully performed on non-ferrous alloys [5–8], steels [9, 10] and composites [11]. The preparation of semisolid slurry with a microstructure consisting of equiaxed grains and continuous liquid films at grain boundaries is essential for subsequent processing [12]. Up to date, several technologies have been used to prepare the semisolid slurry or feedstocks, viz. mechanical

Available online at http://link.springer.com/journal/40195

✉ Kai-Kun Wang
ustbkkwang@126.com

[1] School of Materials Science and Engineering, University of Science and Technology Beijing, Beijing 100083, China

[2] Wuxi Turbine Blade Co., Ltd, Wuxi 214174, Jiangsu, China

and electromagnetic stirring (EMS) [13], ultrasonic vibration [11], cooling slope (CS) [14], strain-induced melting activation (SIMA) [15, 16] and recrystallization and partial remelting (RAP) [17, 18]. Among all the preparation methods, SIMA and RAP receive much more attention owing to the capability of processing various alloys with finer grain morphology and superior mechanical properties as well as the simplicity to perform. The SIMA and RAP processes produce the desirable structures by plastic deformation and a following heat treatment in the mushy zone. In these routes, the materials are warm (SIMA) or cold (RAP) deformed by extrusion (or forge, rolling) and reheated to a temperature between solidus and liquidus and then kept isothermally for a certain period, thus resulting in fine, uniform and non-dendritic spherical microstructure.

In SIMA and RAP, pre-deformation plays an important role in the characteristics of the final product. It is indicated that at least 50% cold working is necessary in order to obtain a uniform and fine microstructures during semisolid heating [19]. An issue occurs, for conventional SIMA and RAP methods in which materials are extruded, rolled or forged before being heated to the semisolid temperature range, inhomogeneity and inadequate of the amount of strain restricts the grain recrystallization and spheroidization processes.

Introducing severe plastic deformation (SPD) in the SIMA route to achieve highly strained structure prior to partial remelting is the most effective way to produce fine equiaxed grains. The ECAP is an especially attractive processing technique because fairly large billets can be prepared by a relatively simple procedure. In addition, large amount of stain can be achieved by multiple passes of ECAP without changing the cross-sectional dimensions of the workpiece after each pass pressing. The investigations and applications of ECAP in producing ultrafine-grained materials have been introduced by Valiev et al. and Zhu et al. [20–22]. In the past few years, the applications of ECAP to aluminum [23, 24], magnesium [25], copper [26] and titanium [27, 28] have been investigated. The influence of channel angle parameters [29], pressing routes [30], pressing temperatures [31], pressing speed [32] and the number of pressing passes [33] on the microstructural evolution and mechanical properties of materials has been reported. All these studies confirm that materials with fine microstructure and excellent mechanical properties can be achieved by suitable ECAP processing parameters.

Combining the ECAP technique and the semisolid processing is a new route for producing thixotropic materials in recent years. Proni et al. [34] processed three kinds of Al–Si-Cu alloys by ECAP prior to semisolid heating. The results showed that all the alloys exhibited good morphological stability in the semisolid state without significant changes in size and shape. Zhao et al. [35] investigated microstructural evolution of an ECAP-formed ZK60-RE magnesium alloy in the semisolid state. It was revealed that solid grains were refined and liquid formation rate was obviously enhanced as the increasing number of ECAP passes. Ashouri et al. [36] and Moradi et al. [37] researched the microstructural evolution of ECAP-processed A356 alloy in semisolid state. It was found that with the increase in strain, sphericity of particles increased, their size was decreased, and spheroidization took place in less reheating time. Aghaie-Khafri et al. [38] investigated the effects of coupling ECAP and heating at semisolid temperature on the microstructure of an Al–Fe–Si alloy. The results showed that this new processing route led to better microstructural stability and enhanced mechanical properties. Meshkabadi et al. [39] investigated the combined effects of ECAP and subsequent heating to a semisolid temperature on the microstructural characteristics of the 7075 Al alloy using experimental tests and Taguchi method. The results showed that the processing route and holding time were the most significant experimental factors on the grain size, while the shape factor was significantly affected by processing routes, holding time and heating temperatures.

The present work aims to employ the ECAP in SIMA process to obtain equiaxed and refined 7075 Al alloy. The influences of the number of ECAP passes, heating temperature and soaking time on the microstructural evolution and tensile properties of 7075 aluminum alloy are investigated in the semisolid state. In addition, the mechanism of grain coarsening and the effect of ECAP on the recrystallization and liquid penetration during the isothermal holding are also analyzed.

2 Experimental

2.1 Materials and Thermal Analysis

The initial material used in this study is commercial extruded cylinder bar of 7075-T6 aluminum alloy, and the composition is shown in Table 1. The liquid fraction–temperature relationship was determined by differential scanning calorimeter (DSC, SDT-Q600). Sample of 20 mg was cut and put into the carbon pans in argon atmosphere. The DSC test was performed with the heating rate 10 °C/min from room temperature to 700 °C and then cooled to room temperature with the same rate. The curve of liquid

Table 1 Chemical composition of as-received 7075 Al alloy (wt%)

Zn	Mg	Cu	Fe	Si	Cr	Mn	Al
6.05	2.48	1.63	0.24	0.15	0.23	0.30	Bal.

fraction versus temperature of 7075 Al alloy by integrating the DSC curve is shown in Fig. 1. The semisolid processing window is approximately 50 °C, with the solid fraction varying from 0.63 (620 °C) to 0.97 (570 °C).

2.2 Homogenization, ECAP Deformation and Partial Remelting

Cylinder specimens with 20 mm in diameter and 70 mm in height were cut from the as-received materials and heated to 475 °C for 120 min to homogenize the microstructure and then the samples were furnace-cooled to room temperature. The homogenized samples were processed by ECAP. The ECAP die was fabricated from H13 steel with two equal cross-section channels (20.5 mm in diameter). The inner and outer arc angles, as shown in Fig. 2a, were $\Phi = 120°$ and $\Psi = 60°$, respectively. The samples and ECAP die were heated at 250 °C for 10 min, and a thermometer was used to monitor the temperature. Molybdenum disulfide (MoS_2) was used as the lubricant to reduce the friction between the billet and the die wall. According to Valiev and Langdon [22], the equivalent strain ε_N for N-pass ($N = 1$–4) ECAP-processed sample was given as:

$$\varepsilon_N = \frac{N}{3}\left[2\cot\left(\frac{\Phi}{2}+\frac{\Psi}{2}\right) + \Psi\mathrm{cosec}\left(\frac{\Phi}{2}+\frac{\Psi}{2}\right)\right] \quad (1)$$

Therefore, equivalent strains of 0.67, 1.34, 2.01, 2.68 were achieved through one to four passes of ECAP, respectively. The pressing speed was 15 mm/s forced by hydraulic press (YT32-200C). After each pass extrusion, the deformed billet was immediately quenched into the cold water to "freeze" the microstructure. In addition, in route Bc the billet was rotated by 90° in the same sense (either clockwise or counterclockwise) between each pass extrusion, as illustrated in Fig. 2b.

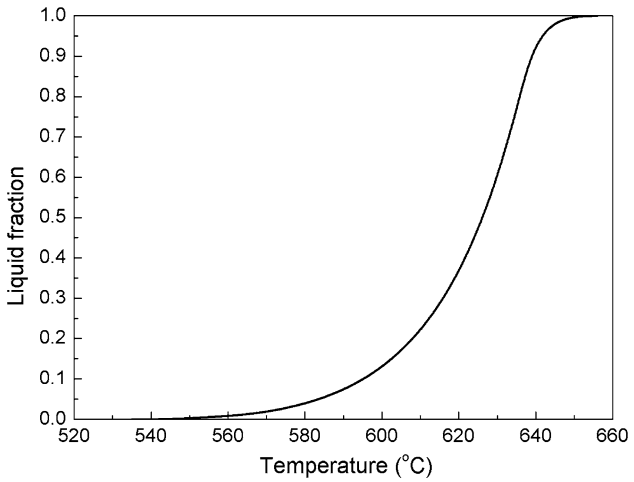

Fig. 1 Curve of liquid fraction versus temperature of 7075 alloy

The ECAP deformed billets were heated to the semisolid temperature. A PID-controlled resistance furnace was used to heat the samples, and the temperature of the samples was monitored by a K-type thermometer. The heating rate was 200 °C/min, and as soon as the samples reached the required temperature, the holding period started. The samples were machined to cylinder configuration with the size of $\phi 10 \times 15$ mm and then isothermally held at 570, 580, 590 and 600 °C for 5–30 min.

2.3 Microstructural Characterization and Tensile Test

The quenched samples after semisolid isothermal treatment were ground up to 3000 grit SiC papers and polished with 0.5 μm diamond paste. Keller reagent (1 ml HF, 1.5 ml HCl, 2.5 ml HNO_3 and 95 ml H_2O) was applied to reveal the specimens' structures. For the following optical microstructural investigation, only transverse section in the center region of the samples was characterized unless otherwise stated.

Optical micrographs (OM) of the specimens were observed using Olympus imager M2 optical microscope. Scanning electron microscope (Zeiss EVO-18) equipped with energy-dispersive spectrometer (EDS) was used to analyze the phase and element distribution. Metallography analysis system was used to quantitatively measure the size and roundness of solid grains, and over 300 particles were calculated for each sample. The average grain diameter D ($D = (4A/\pi)^{1/2}$, where A is the area of the grain) and shape factor F_s ($F_s = 4A\pi/P^2$, where P is the perimeter of the grain) are defined, respectively. X-ray diffraction (XRD) was used to detect the phases in the samples by a Smartlab 9 KW model apparatus with Cu (K_α) target and wavelength of 0.15406 nm.

The tensile test specimens were machined from the quenched samples and prepared according to ASTM E 8 M standards. The tensile specimens were extracted parallel to the extrusion direction. The tensile mechanical properties for 7075 samples under different processing conditions were measured at a strain rate of 1×10^{-3} s^{-1} using an WDW-200D universal testing machine. Each tensile value is the average of three measurements. T6 heat treatment consisting of a solution process (477 °C × 6 h) and a two-stage aging process (120 °C × 3 h + 170 °C × 3 h) was performed on semisolid processed materials with different number of ECAP passes.

3 Results

3.1 Microstructures of As-Received, Homogenized and ECAP Deformed Alloy

The OM image of the transverse microstructure of the as-received 7075 Al alloy is presented in Fig. 3. The

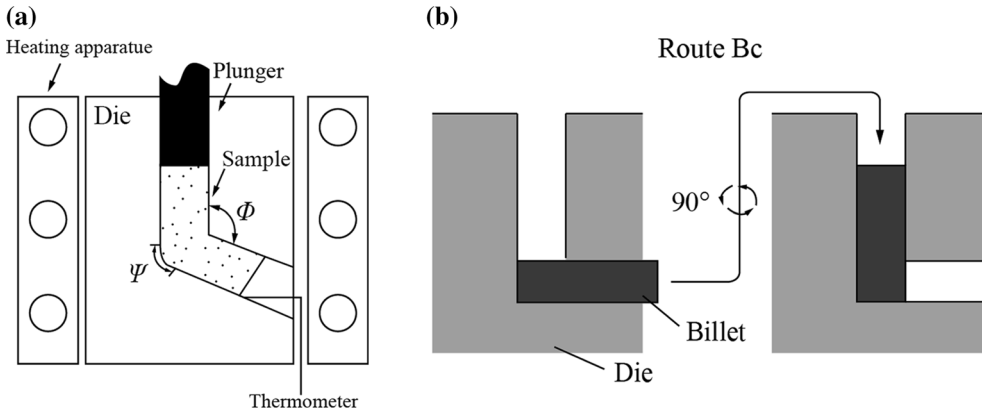

Fig. 2 Schematic illustration of **a** ECAP die, **b** pressing route Bc

microstructure consists of large amounts of unrecrystallized α-Al grains as the matrix and numerous small equiaxed precipitates.

The SEM backscattered electron images of the as-received and homogenized 7075 Al alloys are shown in Fig. 4. In the as-received sample, some precipitate particles with a size of a few hundred nanometers to several micrometers are distributed in the α-Al matrix (Fig. 4a). These precipitates are identified to be Al_2CuMg, Mg_2Si, $Al_2Mg_2Zn_3$ and Al_7Cu_2Fe according to the XRD results (Fig. 5) and other studies [40]. Due to their small content in the microstructure, some of these precipitates were failed to be detected by the XRD analysis (Fig. 5). However, numerous precipitate particles appear and are distributed uniformly in the microstructure after the homogenization treatment (Fig. 4b).

Two kinds of precipitates, viz. the needle-like (indicated by "A") and the block-like (indicated by "B"), can be identified in the homogenized microstructure. The EDS result shown in Table 2 indicates that the needle-like precipitate is the $MgZn_2$ phase. The presence of some Cu content indicates that Zn atoms are substituted by Cu atoms in the $MgZn_2$ phases [40]. The chemical composition in region B reveals that the block-like precipitates are mainly Fe and/or Mn-rich intermetallic compounds. These dispersoids retard the movement of the grain boundaries and make the 7075 alloy very difficult to recrystallize in the solid state [3].

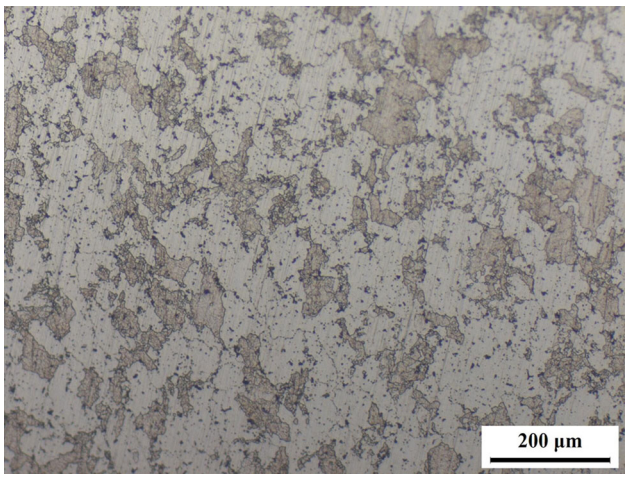

Fig. 3 OM image of transverse microstructure of as-received 7075 Al alloy

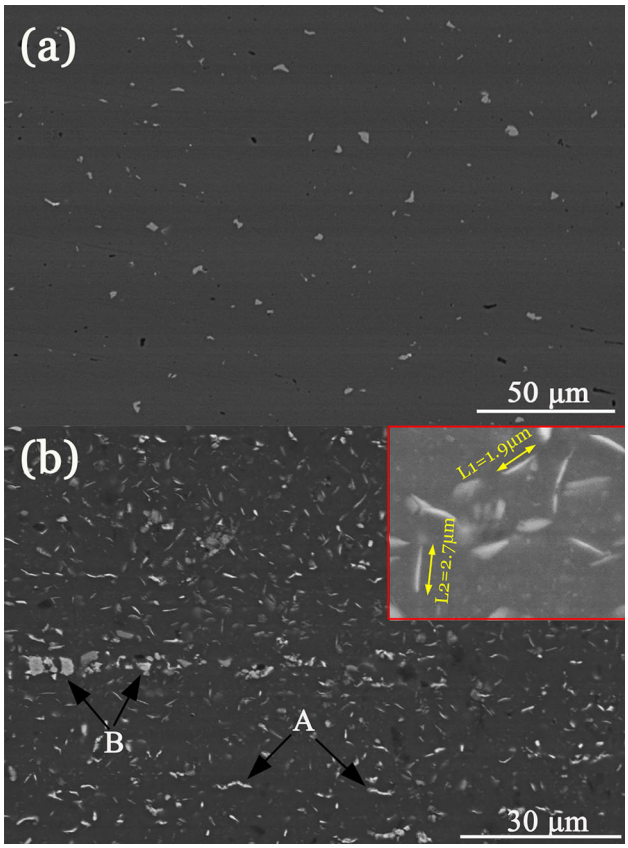

Fig. 4 SEM backscattered electron images of **a** as-received, **b** homogenized 7075 Al alloy (L1 and L2 are the lengths of the needle-like $MgZn_2$ precipitates)

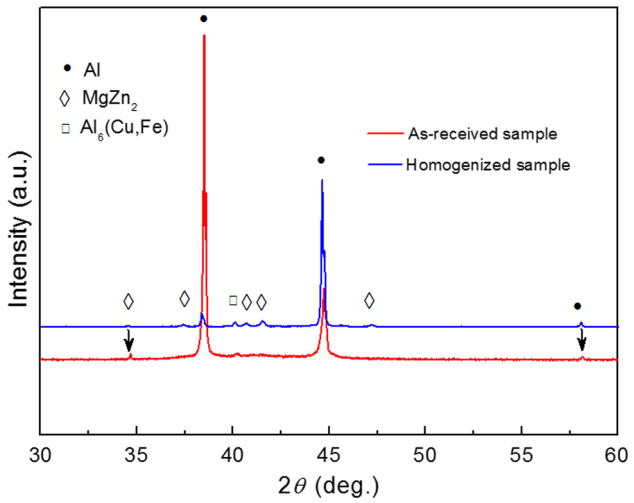

Fig. 5 XRD patterns of as-received and homogenized 7075 alloy

Figure 6 shows the 7075 billets after the four-pass ECAP and the optical graphs. The grains in Fig. 6b were significantly refined after four-pass ECAP deformation comparing with the initial microstructure shown in Fig. 3.

3.2 Microstructural Evolution of ECAP-Processed 7075 Alloy in the Semisolid State

The OM images of the four-pass ECAP-processed 7075 Al alloys followed by isothermal holding at 600 °C for 5–30 min are presented in Fig. 7. The corresponding quantitative values of the average grain size and shape factor are shown in Fig. 8.

It can be observed that both the grain size and shape factor increase with the extension of the holding time. When the duration was 5 min (Fig. 7a), the average grain size is only 18.18 μm and the corresponding shape factor is 0.70. Prolonging the holding time to 10 min (Fig. 7b), most of the solid particles are separated by the liquid film and the grains coarsen to 31.43 μm. Regarding the microstructure of the sample that soaked for 15–25 min, the grains continue to grow and gradually become globular. The average grain size and roundness increase with the increasing holding time. After holding the sample for 30 min, the average grain size ultimately reaches to 74.67 μm and the shape factor increases to 0.87. Therefore, it can be concluded that for the samples holding at 600 °C, the separated grains form after about 5 min, and the increased soaking time contributes to the formation of the more spherical and coarse grains.

3.3 Phase Distribution of ECAP-Processed 7075 Al Alloy in the Semisolid State

The microstructure and X-ray images of the four-pass ECAP-processed 7075 alloy after isothermal treatment at 600 °C for 10 min are shown in Fig. 9. The semisolid microstructure mainly consists of isolated solid grains (indicated by 'A'), liquid film at the grain boundaries (indicated by 'B') and liquid droplets within the grains (indicated by 'C'). In addition, some precipitate particles (indicated by 'D') are present around the grain boundaries. The EDS result (Table 3) indicates that region A is the Al matrix where some Mg and Zn atoms are dissolved into the Al crystal. The liquid at the grain boundaries (Region B) and entrapped liquid droplets within the solid grains (Region C) show similar chemical composition. Furthermore, some Si and Fe-rich precipitates are found at the grain boundaries. These phases are hard to deform and usually display an irregular or polygonal shape. The presence of Fe-rich precipitates at the grain boundaries may have a retarding effect on the coarsening process of the solid grains during the semisolid treatment because these compounds may narrow the liquid film thickness and hinder the migration of alloying elements [3].

Based on the results presented in Table 3 and Fig. 9, there is a considerable depletion of Al in the exterior of the grains. Critical segregation of Cu and slight segregation of

Table 2 EDS result of precipitates in homogenized 7075 Al alloy

Element	Region A		Region B	
	Mass fraction (%)	Atomic fraction (%)	Mass fraction (%)	Atomic fraction (%)
Al	69.38	78.92	74.46	84.44
Zn	18.13	9.53	0.00	0.00
Mg	7.39	9.13	0.00	0.00
Cu	5.10	2.42	3.99	1.92
Fe	0.00	0.00	16.03	8.78
Mn	0.00	0.00	2.18	1.22
Si	0.00	0.00	3.34	3.64
Total	100.00	100.00	100.00	100.00

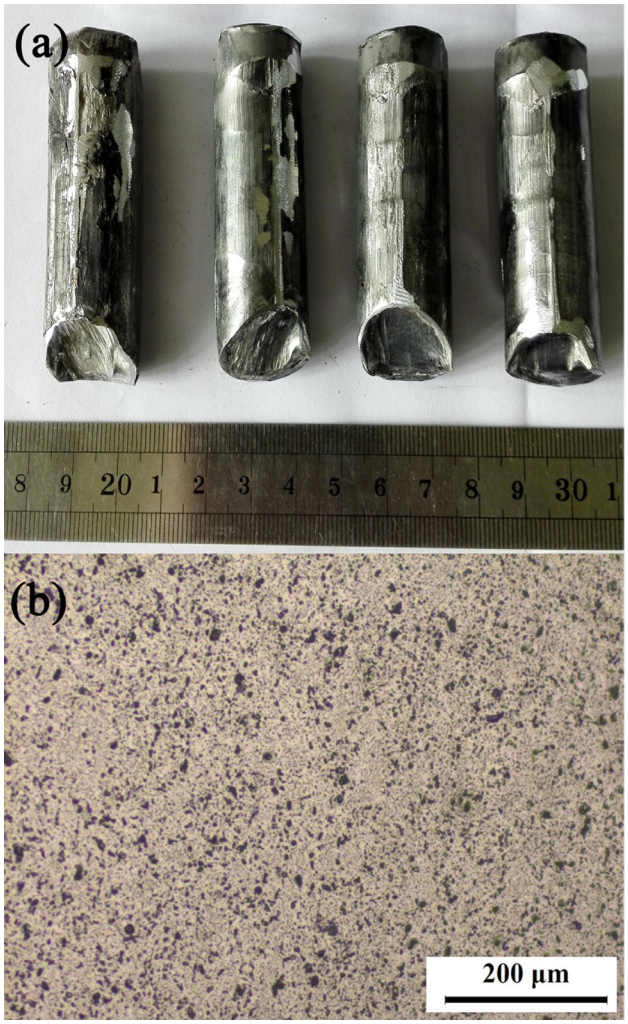

Fig. 6 **a** Four-pass ECAP deformed billets, **b** OM image of the billet

Zn, Mg and Si is observed at the grain boundaries (Fig. 9c–e, g). Fe and Cr are mainly distributed around particular sites, such as in the high melting point phases like intermetallic compound $Al_6(Mn, Fe)$. However, Binesh et al. [41, 42] found a depletion of Mg element at the grain boundaries for the sample held at 600 °C for 35 min. The difference may be due to the inadequate diffusion in this study. Generally, the atomic diffusion is a time-dependent process and the distribution of the alloying elements needs some time to reach the equilibrium state. Mg and Zn are easily dissolved in solid Al, while Cu usually segregates to the grain boundaries. The depletion of alloying elements within the grains increases the melting point of α-Al grains, while the melting point in the exteriors of the grains declines due to the coexistence of large amounts of alloying elements. Moreover, the atomics diffusion promotes the globularization and coarsening process of solid grains and affects the coarsening kinetics of the 7075 Al alloy.

4 Discussion

4.1 Effects of Homogenization on the Microstructural Evolution

As shown in Fig. 4b, large amounts of needle-like $MgZn_2$ precipitates with a length of about 1.5–5 μm and coarse block-like precipitates $Al_6(Cu, Fe)$ and Al_7Cu_2Fe are presented in the microstructure of the homogenized alloys. These precipitates are a few micrometers in size and have a significant influence on the nucleation and recrystallization rates. Binesh and Aghaie-Khafri [42] indicated that these precipitate usually act as the preferential sites for dislocation and recrystallization in the ensuing ECAP deformation process, which is known as the particle-stimulated nucleation (PSN) mechanism. Huang et al. [43] reported that the microstructure with a larger size and higher volume fraction of precipitates showed stronger PSN effect. In the homogenization process, not only the coarse precipitates like $Al_6(Cu, Fe)$, Al_2MgCu and Al_7Cu_2Fe coarsen, but also the $MgZn_2$ phase, are formed and the volume fraction is increased significantly. This makes them preferred nucleation sites for recrystallization during the subsequent deformation and heat treatment. To sum up, the homogenization process of 7075 alloy before the ECAP process leads to a greater number of potential sites for the development of nucleation site and contributes to a fine recrystallized grain size during the semisolid treatment.

4.2 Effects of the Isothermal Time and Temperature on the Microstructural Evolution

According to Fig. 7, it can be concluded that solid grains gradually transform into a globular microstructure when heating the sample at 600 °C. Both the average size and sphericity of the grains increase with the increase in holding time.

Grain coarsening and spheroidization, through surface tension and interface curvature, are two competing processes, and the driving force is to reduce the solid/liquid interfacial energy [44]. Additionally, the coarsening of the solid grains is controlled by different mechanisms for different holding time, as shown in Fig. 10. When the samples are soaked at 590 °C for 15 min (Fig. 10a), coalescence mechanism is dominant whereby two or more solid particles with similar orientation merge into one larger grain (indicated by black arrows). Mohammadi et al. [45] suggested that the grain growth by coalescence by grain boundary migration is dominant at short times after liquid is formed, at low volume fractions of liquid. Bolouri et al. [46] also confirmed that coalescence frequency is

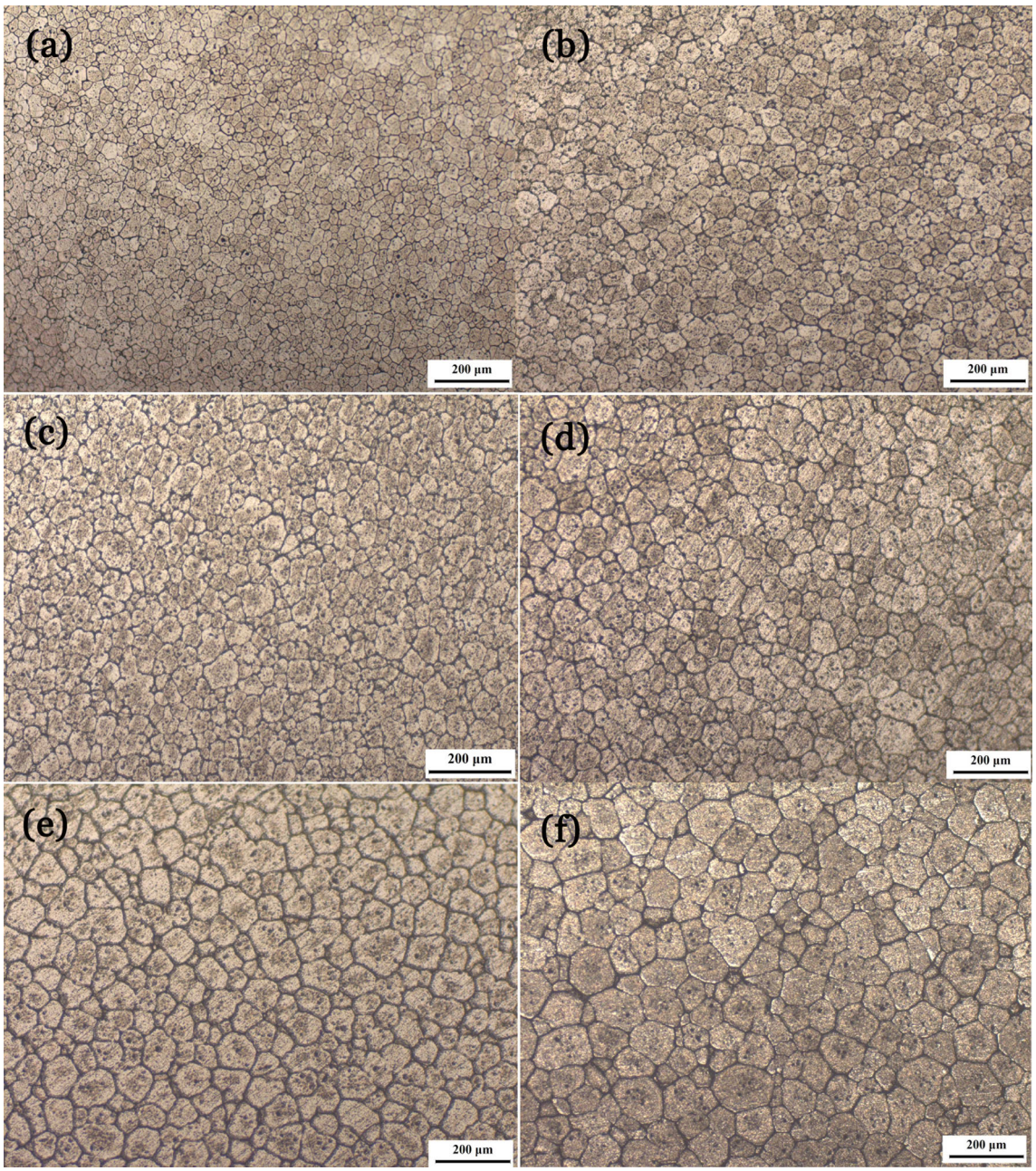

Fig. 7 OM images of four-pass ECAP-processed 7075 Al alloy heating at 600 °C for 5 min (**a**), 10 min (**b**), 15 min (**c**), 20 min (**d**), 25 min (**e**), 30 min (**f**)

associated with the adjacent grain number of each grain and is expected to occur at early stages of heating where the number of necks per grain is relatively high and grains are discrete. However, for the alloys soaked at 590 °C for 30 min (Fig. 10b), most of the solid grains are wetted by the increased liquid fraction. The connecting frequency is reduced and thus leads to the lower activity of the coalescence mechanism. In this regard, the coarsening of the solid grains is mainly controlled by the Ostwald ripening mechanism where the larger grains grow while the smaller ones disappear, as indicated by white arrows. It is worth noting that these two coarsening mechanisms are simultaneously and independently active as soon as the liquid phase forms [12, 16, 45, 46]. The result of the coalescence and Ostwald ripening is the increase in the average grain size, and to some extent, Ostwald ripening contributes to the grain spheroidization.

The effects of isothermal temperature on the microstructural evolution of semisolid 7075 alloy are shown in Fig. 11. It is evident that solid grains gradually

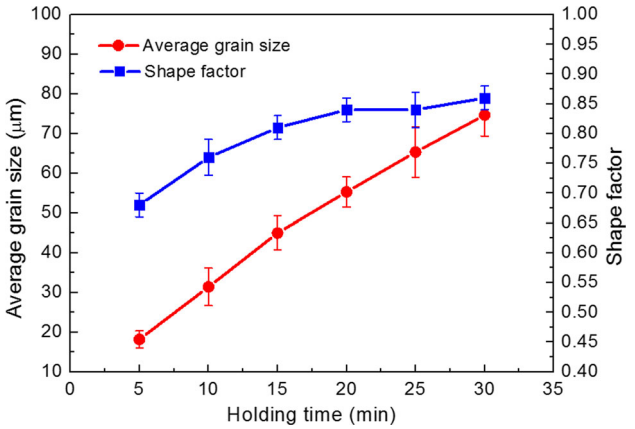

Fig. 8 Variations of average grain size and shape factor with increasing holding time of four-pass ECAP-processed samples heated at 600 °C

transform from irregular particles into globular microstructure by increasing the heating temperatures. For the sample heated at 570 °C (Fig. 11a), most of the grain boundaries are not penetrated by the liquid and large amounts of grains are connected with each other. Additionally, many intermetallic compounds can be found at the grain boundaries, as indicated by red arrows. Following the increased soaking temperature to 580 °C (Fig. 11b), solid grains with irregular shape are formed and the fraction of liquid significantly increases, while the number of secondary phase particles clearly decreases. However, the liquid fraction is still low and parts of the solid grain boundaries are not wetted as indicated by red arrows. Moreover, the grain size exhibits inhomogeneity due to the

Table 3 EDS result for regions A–D shown in Fig. 9a

	Al	Zn	Mg	Cu	Fe	Si
A	94.58	3.40	2.02	–	–	–
B	57.23	12.43	12.61	17.73	–	–
C	82.46	6.64	5.46	5.44	–	–
D	80.87	3.78	3.32	–	4.05	7.99

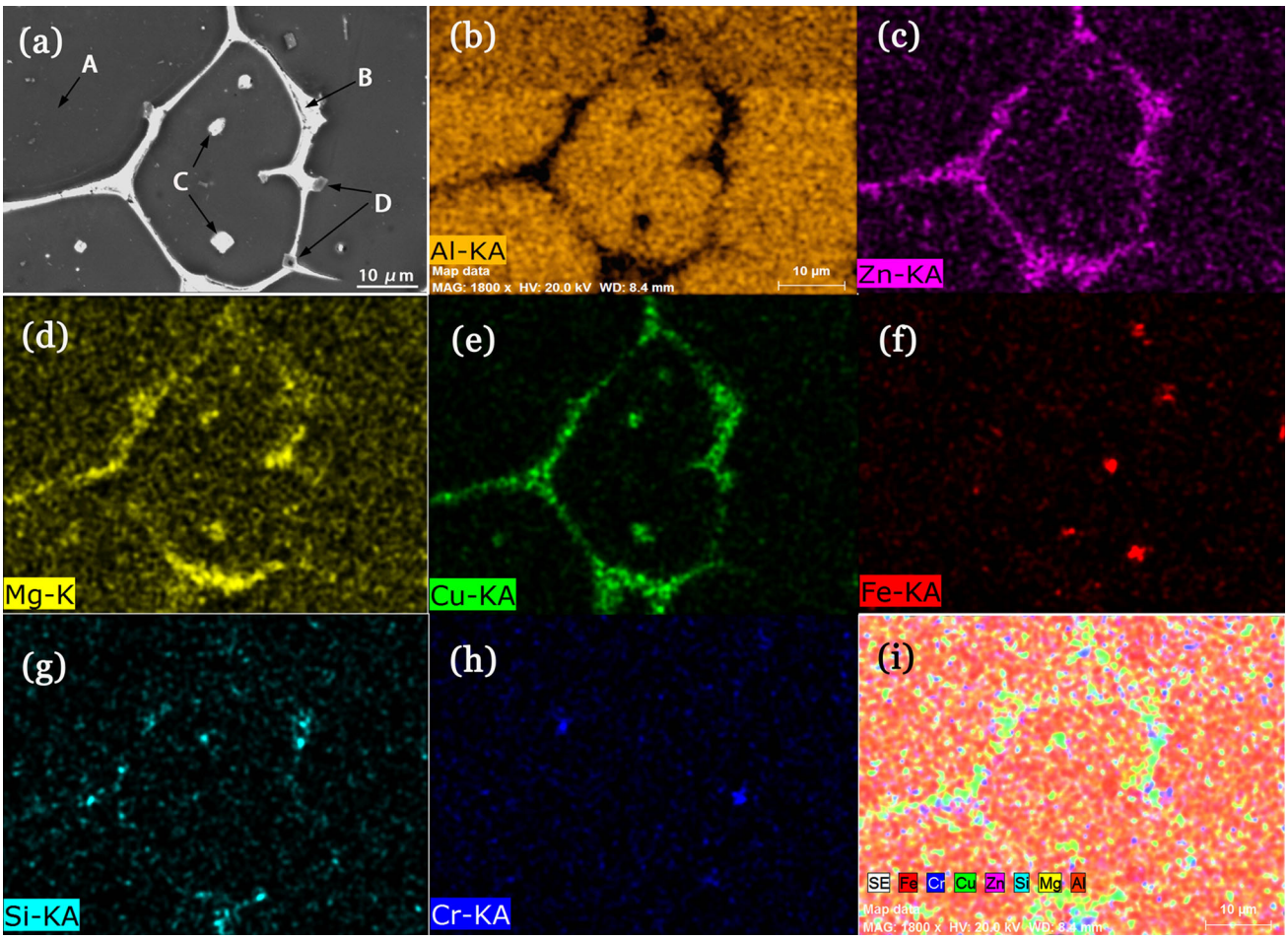

Fig. 9 **a** SEM image, **b** Al, **c** Zn, **d** Mg, **e** Cu, **f** Fe, **g** Si, **h** Cr, **i** all elements X-ray image analyze of four-pass ECAP-processed 7075 Al alloy reheated at 600 °C for 10 min

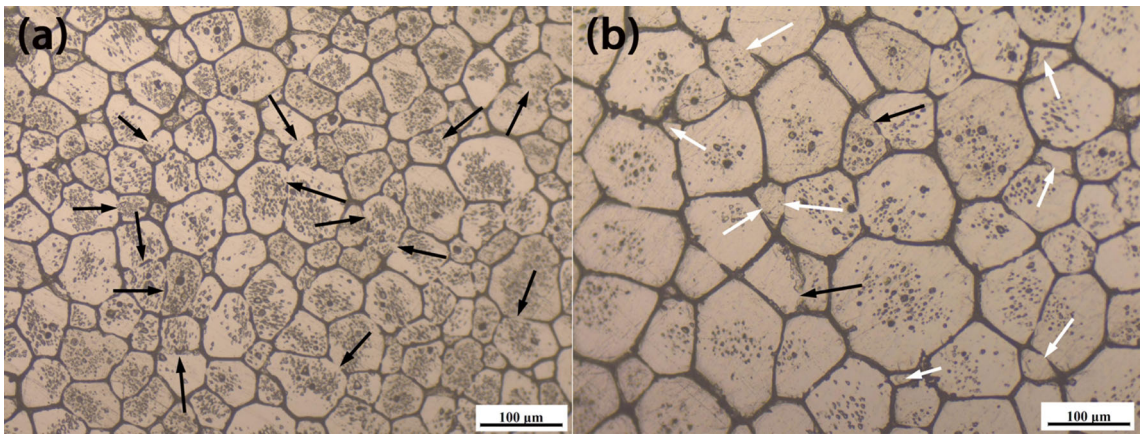

Fig. 10 OM images of semisolid microstructures for one-pass ECAP-processed 7075 alloys after soaked at 590 °C for 15 min (**a**), 30 min (**b**)

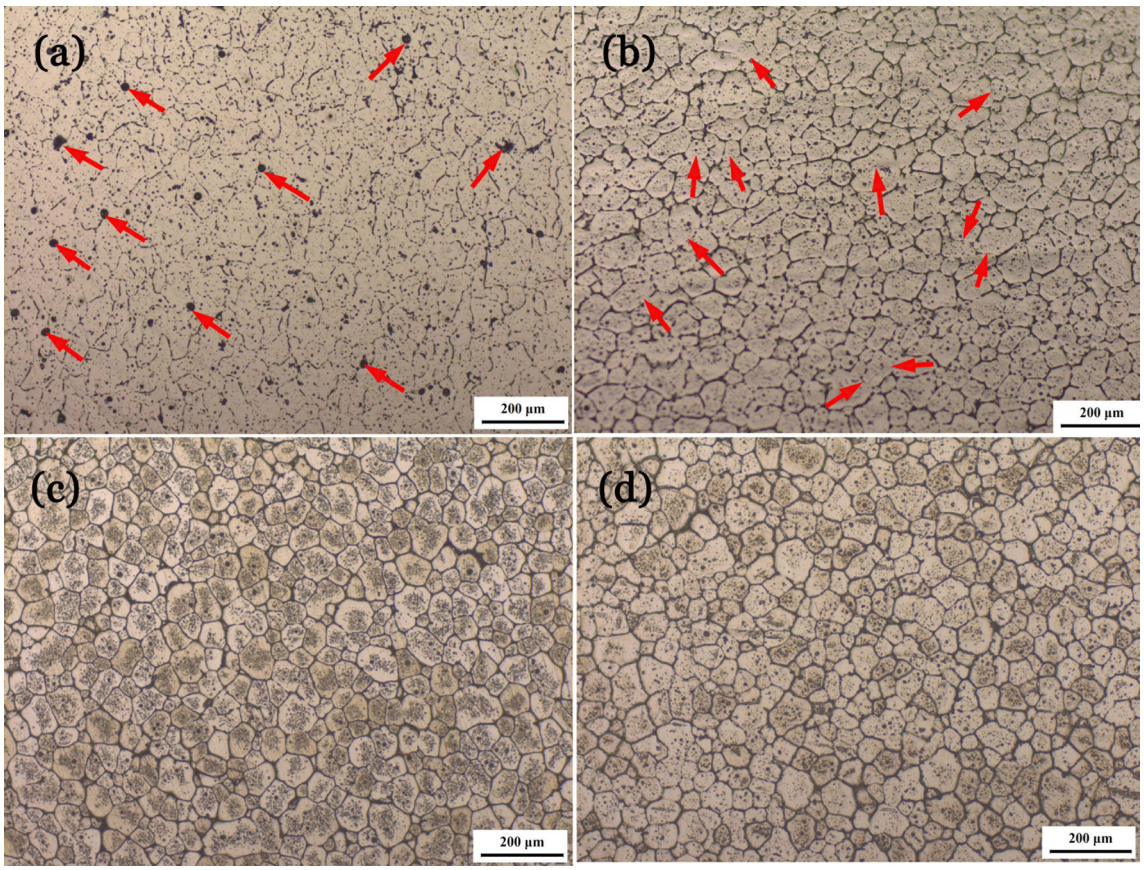

Fig. 11 OM images of semisolid microstructures of one-pass ECAP-processed 7075 Al alloy holding for at 570 °C (**a**), 580 °C (**b**), 590 °C (**c**), 600 °C (**d**) for 15 min

incomplete spheroidization. Further increasing the holding temperature to 590 °C (Fig. 11c), the shape of the solid grains becomes much more equiaxed. Almost all the solid grains are separated by the liquid films because of more abundant liquid fraction. Regarding the sample soaked at 600 °C (Fig. 11d), the size of the solid grains slightly increases compared with that at 590 °C while the roundness of the solid grains decreases slightly. This result is also confirmed by Mohammadi et al. [45] who declared that with the increase in temperature, the roundness of the solid particles increases and the shape of the solid particles becomes more globular. In fact, the ascending temperatures increase the liquid fraction directly and provide a thicker diffusion path for the atomic diffusion. Furthermore, some

precipitates that inhibit the grain boundary movement may be dissolved at higher heating temperatures and thus accelerate grain spheroidization and coarsening.

4.3 Effects of ECAP on the Microstructural Evolution

The microstructures of homogenized and ECAP-processed samples subjected to different number passes of ECAP followed by holding at 600 °C for 15 min are displayed in Fig. 12. Also, toward a detailed view concerning the evolution of the refining process, the quantitative values of the average grain size and shape factor of the semisolid treated samples versus different numbers of ECAP passes are depicted in Fig. 13. Specifically, the micrographs show that the ECAP-formed microstructures are completely replaced by the recrystallized and equiaxed grains. Coarse and irregular solid grains can be observed in the microstructure of the zero-pass ECAP-processed sample (Fig. 12a). After the one-pass ECAP processing, the average grain size decreases significantly from 78.09 to 58.89 μm (Fig. 12b). The sphericity of the one-pass ECAP-processed sample appreciably increases from the initial 0.62–0.71. Considering the higher deformation degree, as can be determined from Fig. 12c–e, the average size of the solid grains decreases continuously while the sphericity of grains increases with the increasing ECAP passes. Correspondingly, the average grain size decreases from 55.31 to 44.99 μm, while the shape factor increases from 0.73 to 0.81. Accordingly, the microstructures are considerably refined and became more spherical with the increased ECAP passes.

The main refining and spheroidization during the SIMA process are believed to be the deformation–recrystallization mechanism [42]. In this study, the refinement process can be divided into two stages, namely ECAP deformation and recrystallization. During ECAP deformation, strong shear deformation occurs and large amounts of distortion energies are stored as the form of dislocations, vacancies and lattice defects [45]. This distortion energy provides the driving force for the ensuing recovery and recrystallization processes. A larger number of new equiaxed grains containing much lower dislocation concentration occur preferentially at the areas around the small precipitates, and consequently, the initial particles are totally replaced through the recrystallization process.

Obviously, increasing the degree of pre-deformation not only promotes the grain refinement, but also accelerates the spheroidization of solid grains. The effect of the number of ECAP passes on the grain recrystallization is presented in Fig. 14. The major difference among the two micrographs in Fig. 14a and b is the number of recrystallized grains. For the one-pass ECAP-processed microstructure (Fig. 14a), only a few recrystallized grains (indicated by red arrows) appear, while a sign of subgrain boundary (indicated by blue arrows) formation is found in the interiors of original grains in the microstructure. These substructures are the preferential sites for the formation of recrystallized grains by absorbing the dislocations resulting from dislocation movement and rearrangement [44]. Increasing the ECAP passes to three (Fig. 14b), however, much more strain energy is stored in the microstructure and the crushed and dispersed distribution of non-deformable intermetallic compounds also contributes to induce large amounts of nucleation sites for the recrystallization. Shaeri et al. [47] suggested that the ECAP process facilitates the nucleation rate for recrystallization by increasing the formation of suitable nucleation sites. In this regard, the rate of grain recrystallization is promoted, which leads to the decrease in the equilibrium size of recrystallized grains and greater number of grain boundaries. Yan et al. [48] also found that higher compression ratio leads to greater the overall grain boundaries and subgrain boundaries area and thus greater potentiality for the development of recrystallized nuclei. Thus, the nucleation rate is increased, which can also result in finer recrystallized grains.

The amount of strain induced by plastic deformation in the structure also has great influence on the globularization of the microstructure during the partial remelting. In fact, the spheroidization is well associated with the atomic diffusion of the alloying elements. The smaller grain size of the microstructure with greater value of pre-deformation degree shortens the diffusion distance and thus the spheroidization process is promoted.

Wang et al. [18, 49] indicated that the RAP and SIMA route can produce finer and more spheroidized semisolid microstructure under the similar isothermal holding condition compared with the semisolid thermal transformation route and as-cast alloy. However, Yan et al. [48] and Bolouri et al. [46] found that the average particle size does not obviously decrease when the compression ratio is higher than 30%. Therefore, a four-pass ECAP is adequate for the microstructure refinement and spheroidization in this study.

According to the above discussion, extrusion passes, holding time and temperatures have significant influence on the final microstructure of the as-deformed alloys after the semisolid treatments. In general, the final microstructure in the semisolid state is the result of the equilibrium of two opposite and independent processes, viz. the refining (deformation–recrystallization) and the growth (coarsening) processes. Although longer holding time improves the roundness of solid grains, too long holding time should be avoided because excessive grain

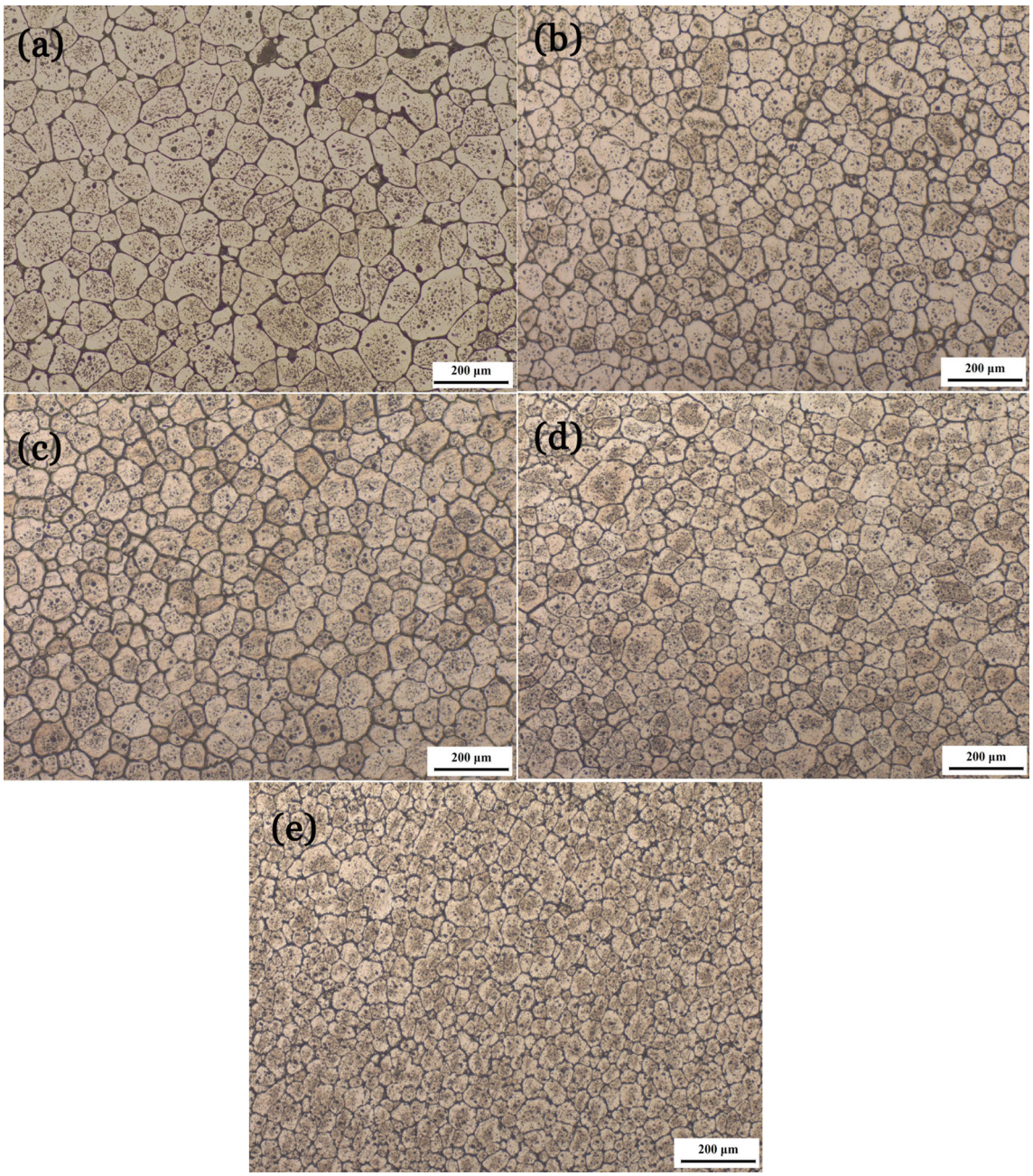

Fig. 12 Effects of extrusion passes on microstructures of ECAP-processed 7075 Al alloy held at 600 °C for 15 min: **a** zero-pass; **b** one-pass; **c** two-pass; **d** three-pass; **e** four-pass

coarsening is detrimental to the thixotropic properties of the products. Therefore, it can be concluded from the partially remelting results that the proper semisolid microstructure with fine and spherical solid grains can be obtained when the 7075 Al alloy is subjected to a four-pass ECAP and reheated at 600 °C for 10–15 min. The average grain size and shape factor vary in the range of 31.43–44.99 μm and 0.76–0.81, respectively.

4.4 Effects of ECAP on the Tensile Properties

The effects of ECAP passes on the tensile properties are shown in Table 4. In addition, the as-received samples (as-extruded and T6) are listed as the reference. Both the 7075 samples after semisolid isothermal treatment (SSIT) with or without T6 treatment show a significant improvement for the yield strength and ultimate strength by increasing the number of ECAP passes from one to four. A slight

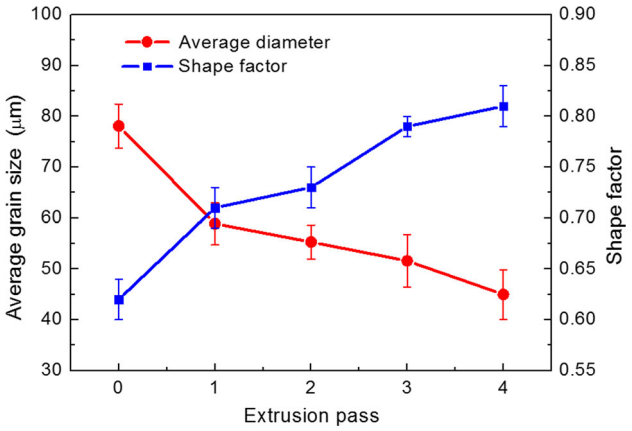

Fig. 13 Variations of average grain size and shape factor versus the ECAP passes for samples heated at 600 °C for 15 min

reduction can be found in the elongation for the four-pass ECAP deformed samples comparing with the one-pass ECAP deformed ones. According to the discussed results, the average grain size of the semisolid microstructure significantly decreases with the increasing number of ECAP passes. Therefore, fine grain strengthening may be the dominant strengthening mechanism for the semisolid 7075 Al alloy in this paper. In comparison with the as-received sample, the 7075 alloy after four-pass ECAP, semisolid treatment and T6 shows a 43% increase in the elongation although there is a slight decrease for the strength. Duan et al. [50] found that yield strength and tensile strength were remarkably increased after 7 ECAP passes. Cardoso et al. [23] also found that there is about 10–15% improvement in the yield strength resulting from ECAP, when compared to the initial samples, while the elongation seems to slightly decrease after the third pass ECAP deformation. The excellent mechanical properties after ECAP processing can be ascribed to precipitation strengthening, dislocation strengthening and fine grain strengthening.

In the partially remelting of deformed 7075 alloy, the segregation of alloying elements, as indicated in Fig. 9, can affect the mechanical properties of the components. For example, Cu and Mg segregate into the interglobular eutectic phase during isothermal soakage in the semisolid state and result in the degradation of the mechanical properties. An improvement of the tensile properties achieved by applying post-heat treatment has been reported for semisolid wrought aluminum alloys [23, 50, 51]. However, Bolouri et al. [52] suggested that the tensile properties of semisolid processed alloys are significantly influenced by the structural properties of the coexisting phases, such as skeletons and interface condition between two coexisting phases. Therefore, a permanent change may not be compensated by any of the post-heat treatments.

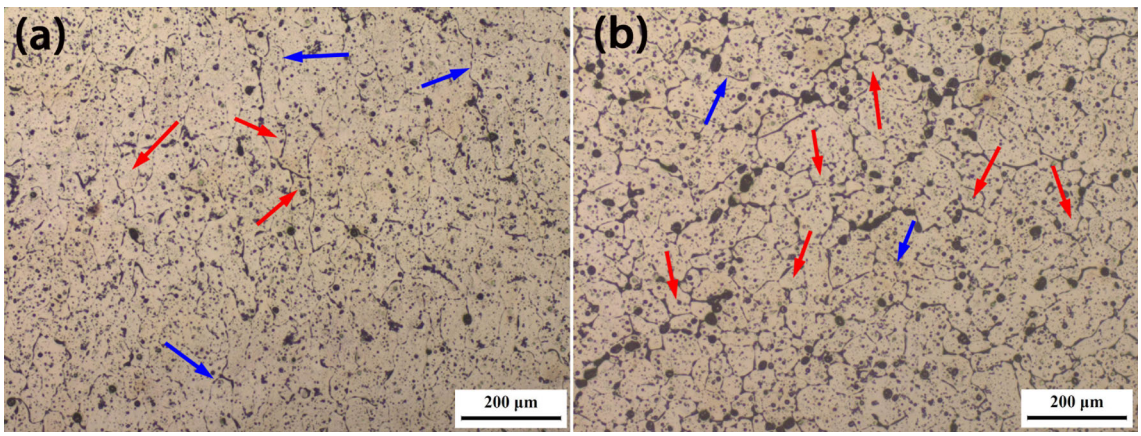

Fig. 14 OM images of semisolid microstructures for ECAP-processed 7075 alloys after isothermal soakage at 570 °C for 5 min: **a** one-pass ECAP; **b** three-pass ECAP

Table 4 Tensile properties of 7075 alloy under different processing conditions (dispersion ± 5% for strength and ± 10% for elongation)

Sample processing	Yield strength (MPa)	Ultimate strength (MPa)	Elongation (%)
As-received (As-extruded + T6)	511	546	9.3
One-pass ECAP + SSIT	178	243	–
One-pass ECAP + SSIT + T6	462	499	14.7
Four-pass ECAP + SSIT	201	268	–
Four-pass ECAP + SSIT + T6	493	541	13.3

5 Conclusions

In this study, ECAP was conducted in the modified SIMA method to prepare the semisolid 7075 alloy. The influences of the number of ECAP passes and subsequent semisolid treatment parameters on the microstructural evolution were investigated. The following conclusions can be obtained according to the above discussion.

(1) Fine and spherical solid grains surrounded by uniform liquid film can be successfully obtained by a modified SIMA route containing homogenization, ECAP deformation and subsequent semisolid soaking. Microstructure observation shows that four-pass ECAP, followed by an isothermal holding at 600 °C for 10–15 min, can be considered as an optimum condition for the semisolid processing parameters wherein the average grain size and shape factor vary between 31.43–44.99 μm and 0.76–0.81, respectively.

(2) The overall trend of the microstructure evolution is that the average grain size increases with the increasing heating temperatures and the decreasing number of ECAP passes. The sphericity of globular particles increases with increasing both temperatures and number of ECAP passes.

(3) A SPD deformation–recrystallization mechanism plays a dominant role in refining the microstructure. The solid grains experience the coarsening and spheroidization processes as soon as the eutectic phases form to minimize the interfacial energy. Coalescence is the dominant mechanism for grain coarsening in the early stage of melting and the Ostwald ripening is active for the longer holding time.

(4) Increasing the number of ECAP passes improves the tensile strength of the globular and heat treated samples due to the grain refining strengthening mechanism. Suitable post-heat treatment improves the mechanical properties of semisolid materials.

Acknowledgements This work was supported financially by the National Natural Science Foundation of China (Nos. 51174028 and 51541406).

References

[1] P.K. Rout, M.M. Ghosh, K.S. Ghosh, Mater. Charact. **104**, 49 (2015)
[2] Ł. Rogal, J. Dutkiewicz, H.V. Atkinson, L. Lityńska-Dobrzyńska, T. Czeppe, M. Modigell, Mater. Sci. Eng. A **580**, 362 (2013)
[3] H.V. Atkinson, K. Burke, G. Vaneetveld, Int. J. Mater. Form. **1**, 973 (2008)
[4] G. Hirt, R. Cremer, T. Witulski, H.C. Tinius, Mater. Des. **18**, 315 (1997)
[5] J.L. Fu, K.K. Wang, X.W. Li, H.K. Zhang, Int. J. Miner. Metall. Mater. **23**, 1404 (2016)
[6] R.G. Guan, Z.Y. Zhao, X. Wang, C.G. Dai, C.M. Liu, Acta Metall. Sin. (Engl. Lett.) **26**, 293 (2013)
[7] X.G. Hu, Q. Zhu, H.X. Lu, F. Zhang, D.Q. Li, S.P. Midson, J. Alloys Compd. **649**, 204 (2015)
[8] W.Y. Jiang, T. Chen, L.P. Wang, Y.C. Feng, Y. Zhu, K.F. Wang, J.P. Luo, S.W. Zhang, Acta Metall. Sin. (Engl. Lett.) **26**, 473 (2013)
[9] E. Becker, V. Favier, R. Bigot, P. Cezard, L. Langlois, J. Mater. Process. Technol. **210**, 1482 (2010)
[10] Y. Meng, S. Sugiyama, J. Yanagimoto, J. Mater. Process. Technol. **225**, 203 (2015)
[11] S.L. Lv, S.S. Wu, C. Lin, P. An, Acta Metall. Sin. (Engl. Lett.) **27**, 862 (2014)
[12] E. Tzimas, A. Zavaliangos, Mater. Sci. Eng. A **289**, 228 (2000)
[13] E.J. Zoqui, J.I. Gracciolli, L.A. Lourençato, J. Mater. Process. Technol. **198**, 155 (2008)
[14] H.M. Guo, X.J. Yang, B. Hu, Acta Metall. Sin. (Eng. Lett.) **19**, 328 (2006)
[15] A. Bolouri, M. Shahmiri, C.G. Kang, J. Alloys Compd. **509**, 402 (2011)
[16] A. Haghparast, M. Nourimotlagh, M. Alipour, Mater. Charact. **71**, 6 (2012)
[17] Z.D. Zhao, Q. Chen, S.H. Huang, F. Kang, Y.B. Wang, Trans. Nonferrous Metals Soc. China **20**, 1630 (2010)
[18] C.P. Wang, Y.Y. Zhang, D.F. Li, H.S. Mei, W. Zhang, J. Liu, Trans. Nonferrous Metals Soc. China **23**, 3621 (2013)
[19] S.Y. Lee, J.H. Lee, Y.S. Lee, J. Mater. Process. Technol. **111**, 42 (2001)
[20] R.Z. Valiev, R.K. Islamgaliev, I.V. Alexandrov, Prog. Mater Sci. **45**, 103 (2000)
[21] R.Z. Valiev, T.G. Langdon, Prog. Mater Sci. **51**, 881 (2006)
[22] Y.T. Zhu, T.C. Lowe, T.G. Langdon, Scr. Mater. **51**, 825 (2004)
[23] K.R. Cardoso, D.N. Travessa, W.J. Botta, A.M. Jorge Jr., Mater. Sci. Eng. A **528**, 5804 (2011)
[24] S.R. Kumar, K. Gudimetla, P. Venkatachalam, B. Ravisankar, K. Jayasankar, Mater. Sci. Eng. A **533**, 50 (2012)
[25] L.L. Tang, Y.H. Zhao, R.K. Islamgaliev, Chi Y.A. Tsao, R.Z. Valiev, E.J. Lavernia, Y.T. Zhu, Mater. Sci. Eng. A **670**, 280 (2016)
[26] J. Wongsa-Ngam, H.M. Wen, T.G. Langdon, Mater. Sci. Eng. A **579**, 126 (2013)
[27] L.Q. Wang, X.T. Wang, L.C. Zhang, W.J. Lu, Mater. Sci. Eng. A **645**, 99 (2015)
[28] Z.J. Lin, L.Q. Wang, X.B. Xue, W.J. Lu, J.N. Qin, D. Zhang, Mater. Sci. Eng. C **22**, 4551 (2013)
[29] N. Serban, N. Ghiban, V.D. Cojocaru, JOM **65**, 1411 (2013)
[30] M. Furukawa, Y. Iwahashi, Z. Horita, M. Nemoto, T.G. Langdon, Mater. Sci. Eng. A **257**, 328 (1998)
[31] A. Yamashita, D. Yamaguchi, Z. Horita, T.G. Langdon, Mater. Sci. Eng. A **287**, 100 (2000)
[32] P.B. Berbon, M. Furukawa, Z. Horita, M. Nemoto, T.G. Langdon, Metall. Mater. Trans. A **30**, 1989 (1999)
[33] N. Serban, V.D. Cojocaru, M. Butu, JOM **64**, 607 (2012)
[34] C.T.W. Proni, L.V. Torres, R. Haghayeghi, E.J. Zoqui, Mater. Charact. **118**, 252 (2016)
[35] Z.D. Zhao, Q. Chen, Y.B. Wang, D.Y. Shu, Mater. Sci. Eng. A **506**, 8 (2009)
[36] S. Ashouri, M. Nili-Ahmadabadi, M. Moradi, M. Iranpour, J. Alloys Compd. **466**, 67 (2008)
[37] M. Moradi, M. Nili-Ahmadabadi, B. Poorganji, B. Heidarian, M.H. Parsa, T. Furuhara, Mater. Sci. Eng. A **527**, 4113 (2010)
[38] M. Aghaie-Khafri, D. Azimi-Yancheshme, JOM **64**, 585 (2012)
[39] R. Meshkabadi, G. Faraji, A. Javdani, V. Pouyafar, Trans. Nonferrous Metals Soc. China **26**, 3091 (2016)

[40] B. Binesh, M. Aghaie-Khafri, Metals **6**, 1 (2016)
[41] B. Binesh, M. Aghaie-Khafri, Mater. Charact. **106**, 390 (2015)
[42] B. Binesh, M. Aghaie-Khafri, Mater. Des. **95**, 268 (2016)
[43] H. Huang, Z. Tang, Y. Tian, G. Jia, J. Niu, H. Zhang, J. Pei, G. Yuan, W. Ding, Mater. Des. **86**, 788 (2015)
[44] Y. Xu, L.X. Hu, J.B. Jia, B. Xu, Mater. Charact. **118**, 309 (2016)
[45] H. Mohammadi, M. Ketabchi, A. Kalaki, J. Mater. Eng. Perform. **20**, 1256 (2011)
[46] A. Bolouri, M. Shahmiri, E.N.H. Cheshmeh, Trans. Nonferrous Metals Soc. China **20**, 1663 (2010)
[47] M.H. Shaeri, M. Shaeri, M.T. Salehi, S.H. Seyyedein, M.R. Abutalebi, Prog. Nat. Sci. Mater. Int. **25**, 159 (2015)
[48] G.H. Yan, S.D. Zhao, S.Q. Ma, H.T. Shou, Mater. Charact. **69**, 45 (2012)
[49] C.P. Wang, H.S. Mei, R.Q. Li, D.F. Li, L. Wang, J. Liu, Z.H. Hua, L.J. Zhao, F.F. Pen, H. Li, Acta Metall. Sin. (Engl. Lett.) **26**, 149 (2013)
[50] Y.L. Duan, L. Tang, G.F. Xu, Y. Deng, Z.M. Yin, J. Alloys Compd. **664**, 518 (2016)
[51] R. Ghiaasiaan, X.C. Zeng, S. Shankar, Mater. Sci. Eng. A **594**, 260 (2014)
[52] A. Bolouri, C.G. Kang, J. Alloys Compd. **516**, 192 (2012)